Bioresource Technology 300 (2020) 122708

Contents lists available at ScienceDirect

Bioresource Technology

journal homepage: www.elsevier.com/locate/biortech

Microbial aging of hydrochar as a way to increase cadmium ion adsorption capacity: Process and mechanism

Yun Hua[b,c,1], Xuebo Zheng[a,1], Lihong Xue[b,f], Lanfang Han[d], Shiying He[b], Tripti Mishra[b], Yanfang Feng[b,e,f,*], Linzhang Yang[b], Baoshan Xing[e]

[a] Key Laboratory of Tobacco Biology and Processing, Ministry of Agriculture and Rural Affairs, Tobacco Research Institute of Chinese Academy of Agricultural Sciences, Qingdao 266101, China
[b] Key Laboratory of Agro-Environment in Downstream of Yangtze Plain, Ministry of Agriculture and Rural Affairs, Institute of Agricultural Resources and Environment, Jiangsu Academy of Agricultural Sciences, Nanjing 210014, China
[c] College of Resources and Environment Science, Nanjing Agricultural University, Nanjing 210095, China
[d] Institute of Environmental and Ecological Engineering, Guangdong University of Technology, Guangzhou 510006, China
[e] Stockbridge School of Agriculture, University of Massachusetts, Amherst, MA 01003, USA
[f] School of the Environment and Safety Engineering, Jiangsu University, Zhenjiang 212001, China

GRAPHICAL ABSTRACT

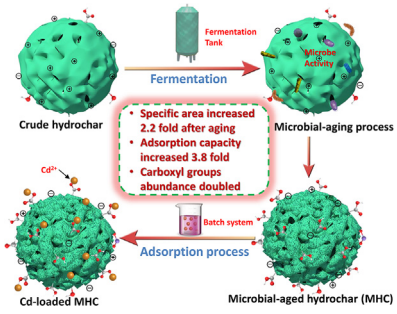

ARTICLE INFO

Keywords:
Sawdust hydrochar
Microbially aged process
Cadmium
Adsorption mechanisms
Biochar aging

ABSTRACT

Microbially-aged hydrochar were prepared to investigate how aging affected their ability to remove Cd^{2+} from aqueous solutions. Based on aging time in an anaerobic fermenter, four samples were produced: HC, M20-HC, M40-HC, and M60-HC. Results indicated increases in specific surface area, pH, and negative charge on hydrochar surface with aging process. Also, there were a decrease in O/C and an increase in surface functional groups, such as –COOH. The adsorption experiments confirmed the positive correlation between aging time and adsorption performance. The 60-day-aged M60-HC treatment displayed the maximum adsorption capacity, which was 3.8 times higher than that of HC. The Langmuir and pseudo-second-order kinetic equations fitted well with isothermal and kinetic data, respectively. Thermodynamic study indicated that Cd^{2+} adsorption is dominated by chemisorption. This study showed that microbial aging process is an effective and promising measure to improve hydrochar adsorption capacity for Cd^{2+}.

* Corresponding author at: Zhongling St. 50, Xuanwu District, Nanjing, Jiangsu Province 210014, China.
E-mail address: jaasfengyanfang@163.com (Y. Feng).
[1] These authors contributed equally to this paper.

https://doi.org/10.1016/j.biortech.2019.122708
Received 29 October 2019; Received in revised form 24 December 2019; Accepted 27 December 2019
Available online 31 December 2019
0960-8524/

1. Introduction

Cadmium, a toxic heavy metal, is usually found in cationic form (Cd^{2+}) in the wastewater discharged from batteries, ceramic, paint, electroplating, mines, phosphate fertilizers, and other industrial processes and products (Fosso-Kankeu, et al., 2017). Cadmium is extremely toxic to humans and can lead to blood, muscle, bone, urinary tract, and cardiovascular diseases (Cui et al., 2018; Henriques et al., 2019). The most widely used technologies for Cd removal include co-precipitation, ion exchange, membrane separation, filtration/ultrafiltration, reverse osmosis, and dialysis/electrodialysis (Bolisetty et al., 2019).

Every technology has its own application scope and shortcomings. For example, co-precipitation produces a large amount of sludge, resulting in secondary pollution. Technologies like ion exchange, membrane filtration, and electrodialysis are characterized by high operating and maintenance costs. Among the mentioned conventional technologies for Cd removal, adsorption has a good application potential because of its operational simplicity and low-cost (Gayathri et al., 2019). In fact, 2015, the degree of popularity of adsorption technology for Cd removal depends on finding a low-cost and high-efficiency adsorbent.

Biochar is a carbon-rich solid of anthropogenic origin. This product is a low-cost absorbent obtained from the pyrolysis, hydrolysis, gasification, or dissociation of biomass in limited-oxygen conditions. Biochar is mainly derived from widely available agricultural and forestry waste. In recent years, it has attracted much attention as a low-cost heavy metal absorbent because of its high specific surface area and high affinity of their surface functional groups (Wang and Wang, 2019). Yu *et al* found that corn stalk-derived biochar removed 88.1% of Cd^{2+} from sewage samples (Yu et al., 2018).

Hydrochar is a special type of biochar obtained by hydrothermal carbonization of biomass performed in the 150–375 °C temperature range under autogenous pressure (Usman et al., 2019). Hydrothermal carbonization results in the production of a char characterized by the presence of abundant oxygen-containing functional groups (Yu et al., 2019). Parshetti et al found that the carbonaceous material prepared from a lignocellulosic feedstock by hydrothermal carbonization coupled with chemical activation exhibited high performance for CO_2 capture (Parshetti et al., 2015). The advantages associated with hydrochar use consist of its high energy density, high conversion efficiency, lack of a need for pre-drying, and relatively low preparation temperature. Despite the above-mentioned advantages, hydrochar is characterized by a low aromatic hydrocarbon content, poor heat resistance, and low values for specific surface area and porosity (Patel et al., 2016). Therefore, increasing this product's specific surface area and adsorption porosity as well as the number of oxygen-containing surface functional groups is a necessity for its use in environmental remediation.

Some approaches to improve the physicochemical properties of hydrochar are currently being implemented. Commonly used methods to reach this goal include altering hydrochar properties by physical, chemical, and biological means. Physical methods include alternate drying and wetting and freezing and thawing (Zhang et al., 2019). Chemical methods include acid–base treatment, oxidant treatment, use of metal salts, and metal oxidant treatment (Rechberger et al., 2017). Biological methods for the improvement of hydrochar properties include aging techniques like co-composting to improve the surface oxygenic functional groups of biochar.

In the present study, the Cd^{2+} adsorption capacity of biologically improved hydrochar was investigated. Compared to the physical and chemical technologies for hydrochar improvement, biological technologies are low-cost and environmentally friendly. In this study, the surface characteristics of sawdust-derived hydrochar were improved by enhancing microbial activity on hydrochar surface as part of an anaerobic fermentation process. Notably, anaerobic fermentation is a widely used strategy in organic waste treatment and biogas production (Zhao et al., 2019). The biological modification of hydrochar was performed to achieve microbial aging performed over different time intervals. The effects of aging time on the physical and chemical properties of hydrochar, its adsorption characteristics, and the mechanism of Cd^{2+} adsorption were investigated. This study aims to provide theoretical and experimental data in support of the use of hydrochar derived from agricultural and forestry waste to ameliorate heavy metal pollution.

2. Materials and methods

2.1. Hydrochar preparation and modification

Hydrochar was prepared from sawdust in a sealed self-pressured hydrothermal reactor. The reaction was carried out at a temperature of 220 °C using water as the solvent. The hydrochar thus prepared and was dried in an oven and subsequently subjected to microbial aging in an anaerobic fermenter. The aging inoculum was obtained mixing 100 L of biogas slurry and 11 kg of wheat straw in a 150 L anaerobic fermenter. The inoculum thus prepared was then mixed with 3.78 kg of sawdust hydrochar (HC). The pH in the fermenter was kept in the range of 6–8, and after 20 d, 40 d, and 60 d of aging the fermented products were removed from the fermenter, washed, dried, ground, and sieved (0.3 mm). The unmodified and microbially modified hydrochar samples were labeled HC, M20-HC, M40-HC, and M60-HC, according to the aging time (0–60 days), respectively.

2.2. Characterization of different hydrochar samples

The ash content of hydrochar samples was determined by the ignition method. Freshly prepared hydrochar samples with deionized water in a ratio of 1:10 were used to perform pH measurements. The elemental contents of C, N, and H in the hydrochar samples were determined using an elemental analyzer (Varo EL cube, Elementary, Germany). Analyses performed with this instrument involve high catalytic combustion temperature and infrared detection of the product gases (CO_2, H_2, and NO_2). The samples were analyzed by elemental analysis, SEM-EDS, XPS and FTIR. The sample spectra were measured using a FTIR spectrometer (VERTEX70, Bruker, Germany) scanning in the 500–4000 cm^{-1} wavelength range. The elemental composition of the hydrochar surfaces was determined by X-ray photoelectron spectroscopy (XPS) performed with a Thermo ESCALAB250Xi instrument. The Cd^{2+} concentration in the filtrates after the adsorption process was determined by inductively-coupled plasma-atomic emission spectroscopy (ICP-OES, Perkin Elmer, USA).

2.3. Adsorption experiments

2.3.1. Kinetic experiments

An evaluation of the kinetic adsorption parameters of the various hydrochar samples was carried out in batch experiments. In particular, 0.05 g of each adsorbent sample (HC, M20-HC, M40-HC, and M60-HC) was added to a 25 mL aliquot of a 50 $mg{\cdot}L^{-1}$ Cd^{2+} solution at pH = 7. The mixtures were shaken in a mechanical shaker at room temperature; and at pre-determined time intervals (5, 10, 15, 30, 60, and 90 min), aliquots from the shaken mixtures were filtered through a 0.45 μm membrane. The concentration of Cd^{2+} in the various filtrate samples was measured by ICP-OES. The amount of adsorbed heavy metal was calculated as the difference between the initial and final Cd^{2+} concentrations in the filtrate. All the adsorption experiments were performed in triplicates, and the average parameter values are provided.

Lagergren pseudo-first-order and pseudo-second-order kinetic models were used to fit the sorption kinetics data. According to this model, the rate at which adsorption sites fill is proportional to the number of unoccupied sites.

2.3.2. Isotherm adsorption experiments

In these experiments, 0.05 g hydrochar sample were placed in centrifuge tubes containing 50 mL solutions of Cd^{2+} at different

concentrations (10, 20, 30, 40, and 50 mg·L^{-1}). These samples were then filtered through a 0.45 μm membrane after being subjected to oscillation (160 rad·min^{-1}) at 25 °C for 24 h. Langmuir, Freundlich, and Temkin models were used to fit the adsorption isothermal data.

The Langmuir model assumed that the monolayer adsorbed on the uniform surface without interaction. Freundlich model is an empirical one which is often used to describe chemical adsorption on heterogeneous surfaces. Temkin equation considers that when adsorbent interacts with the adsorbed solute to affect the adsorption behavior and process. The specific energy relationship is that the adsorption heat decreases linearly with the adsorbed amount.

2.3.3. Effect of pH on Cd^{2+} adsorption

To investigate the effect of pH on Cd^{2+} adsorption, aliquots of 1 g·L^{-1} biochar were added to 30 mg·L^{-1} Cd^{2+} solutions adjusted to different pH values (2–11) using 0.1 mol·L^{-1} HCl or 0.1 mol·L^{-1} NaOH solutions. The mixtures were shaken at a constant temperature of 25 °C in an oscillator for 24 h (160 rad·min^{-1}) and later filtered. The Cd^{2+} concentration in the various filtrate samples was then measured.

2.3.4. Effect of the temperature on Cd^{2+} adsorption

The temperature effect on the adsorption process was studied under similar experimental conditions as the isothermal adsorption process. The adsorption reaction temperatures tested were 5 °C, 25 °C, and 45 °C and in an oscillator for 24 h (160 rad·min^{-1}) and later filtered. The initial concentration of the liquid was 30 mg·L^{-1}. The Cd^{2+} concentration in the various filtrate samples was then measured.

2.3.5. Effect of competitive ions on Cd^{2+} adsorption

In real environmental applications, competitive adsorption is a common phenomenon that negatively affects the overall performance of an adsorbent. Therefore, the effect of competitive ions on Cd^{2+} adsorption was investigated. The experimental conditions were similar to those of the isothermal adsorption process described above. Three metal ions of different valence, Na^{+}, Ca^{2+}, and Al^{3+} at the concentrations of 0.01 mol·L^{-1}, 0.05 mol·L^{-1}, and 0.1 mol·L^{-1}, respectively, were used to investigate the effect of competitive ions on Cd^{2+} adsorption experiment.

3. Results and analysis

3.1. Effect of aging time on the basic properties of hydrochar samples

After microbial aging, the surface of hydrochar was rougher and the pore structure was well developed, which can be confirmed by SEM pictures (data not shown). As the aging time increased, so did the number of micropores; M40-HC and M60-HC in particular are characterized by compact and well-arranged pores. Importantly, the adsorption potential of hydrochar is expected to increase alongside the number of pores working as active sites of metal ion adsorption. The above-described observations are also in agreement with the results of the BET specific surface area discussed further on in this article (see Fig. 1a and Table 1).

According to the International Union of Pure and Applied Chemistry, the pores of porous materials are divided into micropores (< 2 nm), mesopores (2–50 nm), and macropores (> 50 nm) based on the size. the N_2 adsorption–desorption curves of fresh HC and aged hydrochar M60-HC display the characteristics of I and IV isotherms, suggesting that microporous and mesoporous structures are present on their surfaces, respectively (Yoshida et al., 2018). Based on the data reported in Fig. 1a, BET analysis calculations indicate that the specific surface areas of fresh HC and M60-HC have values of 3.24 m^2·g^{-1} and 10.33 m^2·g^{-1}, respectively. Thus, microbial modification of hydrochar surfaces causes a decrease in pore size and a contemporary increase in pore volume and specific surface area. The specific surface area of microbial-aged biochar M60-HC displays a three-fold increase with respect to that of HC, which will have more sites for Cd^{2+} adsorption in solution.

The observed increase in pore numbers in microbial-aged hydrochar may be due to the release of dissolved organic matter on the surface of the material (Zhu et al., 2019). With aging, these compounds undergo mineralization, rendering the carbon skeleton more porous and increasing the number and volume of pores. The increase in the number and volume of hydrochar pores also causes an increase in specific surface area and adsorption sites. The presence of soluble organic components on the surface of hydrochar samples is also confirmed by the reduction of TOC (Total Organic Carbon) in the leachate of microbial-aged hydrochar. The TOC content in different hydrochar extract water was 451 mg·g^{-1}, 227 mg·g^{-1}, 155 mg·g^{-1}, 100 mg·g^{-1}, respectively, and the content decreases with aging time.

The properties of hydrochar differ from those of the conventional limited-oxygen-conditions pyrolyzed biochar (pyrochar). Hydrochar is similar to soft biochar material, which contains large amounts of decomposable and soluble organic and inorganic components on the surface of the carbon skeleton. These components get easily lost during microbial fermentation, leaving an empty space, and causing an increase in the specific surface area of hydrochar. The pore development and adsorption properties of pyrochar decrease with aging (Jian et al., 2018). Conventional oxygen-limited pyrolyzed biochar produced at high temperature is relatively rigid, as it comprises relatively inert organic and inorganic components. The microbial degradation of the surface components of pyrochar probably reduced the material's specific surface area by blocking the development of pores and adsorption sites.

To understand the role of surface ion exchange in the adsorption process, the metal ions present on the surface of aged hydrochar samples were analyzed. The analysis was conducted to determine the change in the concentrations of common metal ions (Al^{3+}, Ca^{2+}, and Mg^{2+}) as a consequence of the aging process. As can be seen from the data reported in Fig. 1b, Al^{3+}, Ca^{2+}, and Mg^{2+} concentrations increase following microbial aging. The concentration of Al^{3+} in M60-HC is twice as large as that in M20-HC and M40-HC. The observed trend of increasing Ca^{2+} and Mg^{2+} concentrations with aging indicates that these metal ions can be exchanged with Cd^{2+} in the adsorption process (Cui et al., 2016). Zhang et al. have also reported the amount of Cd^{2+} adsorbed on the biochar surface to be equal to the sum of the metallic cations (e.g., K^{+}, Ca^{2+}, Na^{+} and Mg^{2+}) released in the wastewater (Zhang et al., 2019). However, the insignificant amount of Al^{3+} and Ca^{2+} ions released in the same experiment suggests that ion exchange plays a certain role in the adsorption process, but it is not an important leading role (Kumar et al., 2017).

In order to investigate the influence that temperature has on the residual mass and weight of hydrochar, thermogravimetric (TG) and differential thermogravimetry (DTG) analyses were conducted. The largest weight losses for hydrochar are observed at 55 °C, 190 °C, and 340 °C (Fig. 1c). The weight loss peaks at 55 °C and 190 °C may be due to the loss of adsorbed moisture and chemically-bound water, respectively. Sample volatilization and combustion occur mainly above 340 °C, which suggests the loss of volatile and biodegradable organic compounds, including leftover cellulose, hemicelluloses, and their degradation products (Wang et al., 2018). During hydrochar pyrolysis, the degradation of hemicelluloses and cellulose takes place in the 160–180 °C range, when most of the lignin remains stable (Liu et al., 2018).

Comparison of the intensities of the weight loss peaks of M20-HC, M40-HC, and M60-HC to that of HC at 190 °C indicates that the water content of hydrochar decreases as a consequence of the microbial aging process (Fig. 1c). The second stage, hydrochars were observed huge weightlessness peak in combustion stage. These are indicated by the mass loss peaks at 300–464 °C and 300–404 °C. This indicates that the volatiles lose weight and the combustion stage lasts for a short time and the combustion rate is faster, which may be because the volatiles

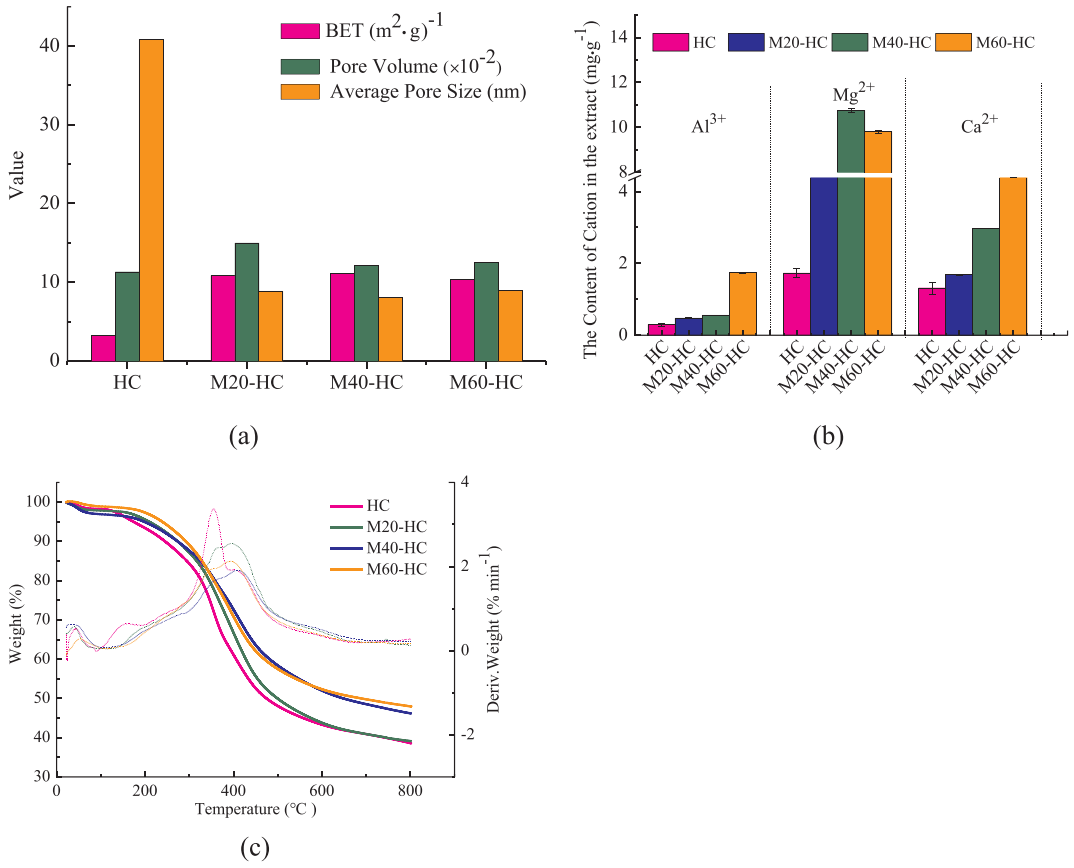

Fig. 1. a) BET, pore volume, and average pore size of HC, M20-HC, M40-HC, and M60-HC; b) metal ion concentrations in hydrochar extracts; c) thermogravimetric (solid lines) and differential thermogravimetry (dotted lines) curves for HC, M20-HC, M40-HC, and M60-HC.

Table 1
Physicochemical properties of hydrochar samples obtained after implementing different aging times.

Parameters	HC	M20-HC	M40-HC	M60-HC
Ash	28.87	26.57	16.78	12.83
pH	4.18	5.17	6.04	6.92
Zeta potential (mv)	0.37	−13.2	−16.3	−18.20
C (%)	63.55	65.36	68.23	67.44
O (%)	30.33	26.48	25.79	25.40
H (%)	2.91	5.63	3.97	3.06
N (%)	2.09	3.47	2.29	2.81
H/C	0.05	0.09	0.06	0.05
O/C	0.48	0.41	0.38	0.38
(O + N)/C	0.51	0.46	0.41	0.42
Al (%)	0.18	0.07	0.34	0.10
Si (%)	0.17	0.29	0.25	0.45
P (%)	1.56	0.11	0.81	0.71
S (%)	0.76	0.27	0.32	0.41
Ca (%)	0.47	0.30	0.47	0.89
Mg (%)	0.33	0.45	0.61	0.69
Fe (%)	1.17	0.36	0.24	0.29
Functional groups (%)	HC	M20-HC	M40-HC	M60-HC
C-C	62.3	28.3	35.8	38.8
C-O	24.1	11.2	42.2	35.2
C = O, COOH	13.6	60.5	22.1	26.2

Note: HC, M20-HC, M40-HC and M60-HC indicate non-aged, and 20 d, 40 d, and 60 d microbially-aged sawdust hydrochar samples, respectively. The content of C, H, O, N was measured by element analysis. The solid-to-liquid ratio of pH was 1:10. The content of Al, Si, P, S, K, Ca, Mg was measured by EDS-Mapping. The content of the zeta potentials (mV) of hydrochar samples were measured at pH = 5. Average abundance of different functional groups was measured by X-ray photoelectron spectroscopy.

content is lower or the required ignition point is not high. The rate of weight loss for M20-HC (2.7%·min^{-1}), M40-HC (2.2%·min^{-1}), and M60-HC (1.9%·min^{-1}) between 300 °C and 464 °C was relatively low compared to the same parameter measured for HC (3.4%·min^{-1}). The low weight loss rates observed for the aged samples confirm the structural stability of hydrochar after undergoing microbial aging. As a carbon fixation material, hydrochar itself needs a stable environment to alleviate the greenhouse effect. At the same time, it can reduce the adverse effects on the adsorption system, such as the release of labile organic components from hydrochar.

The change in the physicochemical properties of the hydrochar as a consequence of microbial aging was studied (Table 1). The ash content of hydrochar was found to decrease gradually with aging (from 28.87% to 12.83%); this effect may be due to the dissolution of mineral components resulting from microbial activity. The pH gradually rises to achieve near-neutral values (from 4.18 to 6.92); this observation may be the result of the microbial decomposition of organic acids present on the surface of hydrochar during aging process. With respect to fresh HC, with aging an increment in C, H, N, and O contents, a decrease in the O/C atomic ratio, and an increase in the H/C and O + N/C atomic ratios were observed (Feng et al., 2019). The results of XPS and FTIR analyses provide further evidence that microbial aging is associated with an increase in the number of oxygen-containing surface functional groups, which causes an increase in the presence of polar functional groups on hydrochar surface (Qian and Chen, 2014).

The zeta potential results indicate that M−HC had a negative charge on its surface and the magnitude of this negative charge increased (from −13.2 mV to −18.2 mV) as a consequence of the aging process. This observed change may be due to an increment in the number of –OH groups on the hydrochar surface. The increase in the number of surface functional groups such as –OH and –COOH also

contributes to the negative surface charge. Notably, the increase in surface negative charge increased hydrochar potential for electrostatic interactions with the positively charged heavy metal ions in solution (Xu et al., 2016).

Results of the SEM-EDS mapping experiments on fresh and aged hydrochar samples indicate that hydrochar surfaces are mainly composed of C, N, O, Ca, Mg, Al, and a small amount of Si. As the aging time of the hydrochar increased, the surface C content decreased, whereas the O, Ca, Mg, Al, and Si contents increased (Table 1). The decrease in surface C content is attributed to the fact that, as aging time increases, the unstable contents dissolves and decomposes under the influence of temperature, moisture, and microbial activity. The rise in O content from 43.83% to 49.56% was also confirmed by XPS and FTIR data, which will be discussed further. The relative increase in the contents of Ca, Mg, Al, and other metallic elements may be due to these elements' resistance to microbial decomposition and degradation.

Silicon is an important constituent of inorganic crystals in biochar (Zama et al., 2018), which, based on SEM-EDS mapping experiments, display a 165% increment following microbial aging. Silicon-based species are difficult to dissolve and decompose. Amorphous phytolith and opal A-particles (phytolith, diatom) are widely present in biomass (Desplanques et al., 2006). In dry weight, biomass may contain 0.1–10% of silicon (Epstein, 2009). Silicon is retained in biomass even after carbonization, and, as a result of aging, it accumulates and gets exposed on the hydrochar surface as insoluble inert silicon. The existence of the Si-O-Si functional group on the hydrochar surface is also confirmed by the peaks observed on the FTIR spectra, as discussed in detail below.

XPS experiments were conducted to investigate the characteristics of the functional groups on the surface of HC, M20-HC, M40-HC, and M60-HC, as well as the mechanism by which Cd^{2+} is adsorbed. By peak splitting (Langova and Matysek, 2010), the bond positions between C–C (284.5 eV), C-O (285.7 eV), C = O (287.0 eV), and –COOH (288.9 eV) were found (Estrade-Szwarckopf, 2004).

After hydrochar microbial aging, the main XPS peak (–COOH) was more obvious at the binding energy of 288.9 eV, indicating that the oxidation degree of hydrothermal carbon increased after aging (see Supporting Information). Table 1 describes the specific changes of the functional groups on the surface of hydrochar samples as a result of microbial aging. A significant increase in the peak of C-O and C = O while the decrease in C–C functional groups was recorded in microbially-aged hydrochar samples. These changes may be attributed to the conversion of surface alkanes to acids or alcohols as part of energy production during anaerobic digestion. The increase in oxygen-containing functional groups, especially C = O and –COOH, has a positive effect on the adsorption of cations like Cd^{2+}. These groups remove heavy metals from the solution by forming metal ion complexes (e.g., R-OH and R-OOH on the carbon surface (Yu et al., 2018).

Results of the FTIR investigation on the surface functional groups of HCs point to the presence of a few absorption peaks at 3338, 2925, 1700, 1600, 1496, 1276, 1205, 1031, 877, 811, and 642 cm^{-1} (see Supporting Information). The position of the –OH absorption peak shifted from 3338 cm^{-1} to 3394 cm^{-1} was observed in the spectra of M20-HC, M40-HC, and M60-HC, and the degree of stretching vibration increased significantly. Additionally, the amplitudes of the peaks attributed to the Si-O-Si stretching vibrations of M20-HC, M40-HC, and M60-HC at 804 cm^{-1} and 1031 cm^{-1} were enhanced, indicating the strengthening of the Si-O-Si bonds of the relevant functional groups present on these hydrochar samples' surfaces (Qian and Chen, 2013).

The characteristics of the infrared spectra of M60-HC recorded before and after performing Cd^{2+} adsorption experiments indicate that, as a consequence of Cd^{2+} adsorption, the –OH absorption peak shifts from 3394 cm^{-1} to 3483 cm^{-1} (see Supporting Information). This shift suggests a weakening of the mentioned bond's stretching vibration. In fact, the formation of a coordination bond between –OH and Cd^{2+} has been reported to reduce the intensity of the intermolecular –OH-based hydrogen bonding interactions (Yu et al., 2018).

After Cd^{2+} adsorption, the degree of telescopic vibration of the aromatic C–H absorption peak at 802 cm^{-1} and 846 cm^{-1} was reduced. This suggests that the aromatic functional groups were involved in the binding of Cd^{2+} (Cortes-Arriagada, 2017). This bonding interaction causes the aliphatic C–H absorption peak at 2934 cm^{-1} to disappear. A shift to 801 cm^{-1} of the absorption peak originally appearing at a wavelength of 781 cm^{-1} indicates that the Si-O-Si functional groups may also act as adsorption sites for Cd^{2+} in the hydrochar. Qian et al (Qian and Chen, 2014) have reported that silicon centers on the biochar surface engage in binding interactions with heavy metal ions to increase the material's adsorption capacity, consistent with the findings of the present study.

The weakening of stretching vibrations of the C = C, C = O, and –COOH bonds as a consequence of Cd^{2+} adsorption confirms the participation of the relevant chemical groups in the adsorption process. Notably, Cd^{2+} has been reported to form complexes with the carboxyl, phenol, hydroxyl, and mercaptan groups (Brose and James, 2013).

3.2. Effect of key environmental parameters on Cd^{2+} adsorption

pH is one of the important parameters for the adsorption performance of heavy metal ions in aqueous solution. It is closely related to the solubility of heavy metal ions, ionization of functional groups on the surface of adsorbent, and electrostatic interaction adsorption site. The data in Fig. 2a indicate that the adsorption of Cd^{2+} increased as the pH shifted from acidic to basic. The Cd^{2+} adsorption by HC, M20-HC, M40-HC, and M60-HC increased 7.96, 3.48, 3.71, and 5.66-fold, respectively, as the pH value went from 2 to 8. In particular, the adsorption capacity slowly increased as the pH value increased from 2 to 5; on the other hand, a rapid increase in this adsorption rate was observed as the pH rose from 5 to 8. In the 2–11 pH range, the largest Q_e values were recorded for M60-HC.

The observed increase in Cd^{2+} adsorption capacity alongside the pH value may be due to the de-protonation of the solution prompted by the increase in pH value (Wu et al., 2017). This phenomenon leads to the development of a net negative charge on the hydrochar surface, which in turn favors Cd^{2+} adsorption (Bai et al., 2017). At pH 6, there are few competitive hydrogen ions, which favors Cd^{2+} adsorption by the surface metal reaction (Aster et al., 2019). At high pH values, a proportion of Cd^{2+} ions are known to form Cd $(OH)_2$, which precipitates from solution, negatively affecting the adsorption capacity of the adsorbent (Rawat and Singh, 2019). Any change or ionic radius deformation also affects the adsorbent's adsorption capacity. However, in the present study, due to the weak acidic nature of hydrochar, Cd^{2+} does not precipitate in Cd $(OH)_2$ form, and the maximum adsorption of Cd^{2+} is recorded at pH 8.

Temperature affects the movement rate of ions in the solution and act on the process of ion adsorption and desorption. The Cd^{2+} adsorption capacity of all hydrochar samples gradually increased as the temperature increased from 278.15 K to 318.15 K (see Fig. 2b). However, the temperature-associated increase in Cd^{2+} adsorption capacity was different for each sample. The said adsorption capacity increased 4.60, 2.35, 1.97, and 1.34 times for HC, M20-HC, M40-HC, and M60-HC, respectively, between 278.15 K and 318.15 K. Thus, both the aging time and temperature have a positive effect on Cd^{2+} adsorption.

The Cd^{2+} adsorption on the adsorbent's surface is an endothermic process, which suggests that, within the appropriate temperature range, the adsorption rate will increase with temperature. The physical reason for the mentioned observation could be that, as the temperature rises, the hydrochar surface particles expand, a phenomenon that causes an increase in the values of the specific surface area and the physical adsorption (Nessim et al., 2011). According to this model, Cd^{2+} adsorption by hydrochar might naturally increase as a consequence of the increase in temperature, so that the summer would be the most favorable time of the year to conduct hydrochar Cd^{2+} adsorption

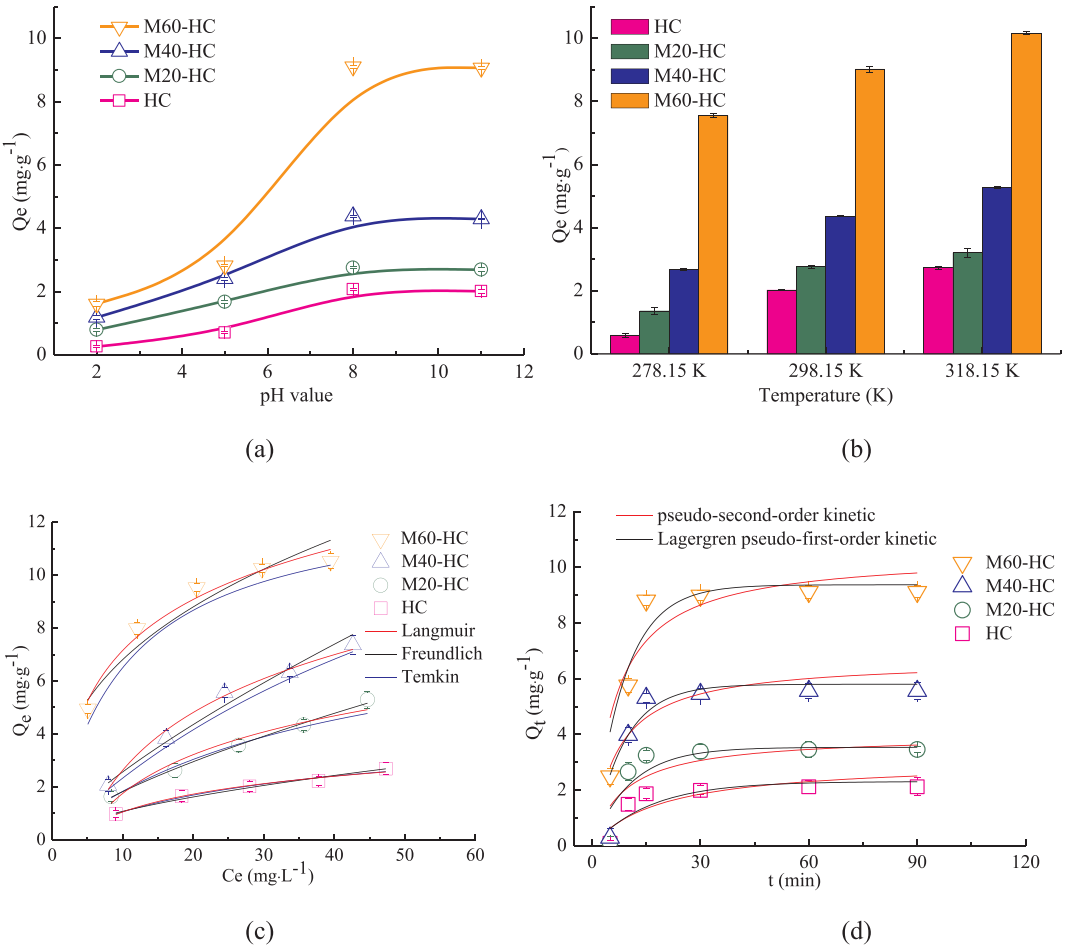

Fig. 2. a) Effect of pH on Cd^{2+} adsorption; b) Effect of temperature on Cd^{2+} adsorption; c) Isothermal plots reflecting the Cd^{2+} adsorption process. Ce means Cd^{2+} equilibrium concentration; Qe means Cd^{2+} equilibrium adsorbing capacity by different hydrochars; d) The adsorption kinetics of the Cd^{2+} adsorption process. Qt means the instantaneous adsorption capacity by unit amount of hydrochar.

Table 2
Effect of competitive ions on Cd^{2+} adsorption by different hydrochar samples.

Ions	Concentration ($mol·L^{-1}$)	$Q_{e,exp}$ ($mg·g^{-1}$)			
		HC	M20-HC	M40-HC	M60-HC
	0 (CK)	1.98 ± 0.02e	2.76 ± 0.04bc	4.56 ± 0.02a	9.02 ± 0.10e
Na^+	0.01	1.59 ± 0.05 cd	2.05 ± 0.11bcd	4.17 ± 0.21e	8.42 ± 0.15bc
	0.05	1.32 ± 0.04bc	1.78 ± 0.14b	3.81 ± 0.09d	6.38 ± 0.19ab
	0.1	0.84 ± 0.04a	0.85 ± 0.05a	2.51 ± 0.13b	4.12 ± 0.16c
Ca^{2+}	0.01	1.78 ± 0.05de	2.66 ± 0.32e	4.14 ± 0.07e	8.79 ± 0.07 cd
	0.05	1.69 ± 0.08d	2.56 ± 0.31de	3.55 ± 0.05c	7.75 ± 0.051b
	0.1	1.18 ± 0.06b	2.04 ± 0.10bcd	3.49 ± 0.03c	6.03 ± 0.10de
Al^{3+}	0.01	1.6 ± 0.30 cd	2.21 ± 0.14bcde	4.12 ± 0.05e	8.73 ± 0.05 cd
	0.05	1.59 ± 0.08 cd	2.45 ± 0.31cde	3.45 ± 0.05c	7.64 ± 0.05bc
	0.1	1.15 ± 0.07b	1.89 ± 0.23b	3.43 ± 0.05c	5.96 ± 0.06d

Note: the competing species were Na^+, Ca^{2+}, and Al^{3+} ions, and the ion concentrations were 0.01 $mol·L^{-1}$, 0.05 $mol·L^{-1}$, and 0.1 $mol·L^{-1}$, respectively. $Q_{e,exp}$ is the experimental equilibrium adsorption value ($mg·g^{-1}$).

procedures. This will be further discussed in section 3.3.2.

The results of adsorption experiments conducted in the laboratory setting are generally different from those carried out in the field, and the reason for this observation lies the presence of competitive coexisting ions in the natural environment. Therefore, the adsorption of Cd^{2+} was tested in the presence of three metal ions that are abundantly present in nature: Na^+, Ca^{2+}, and Al^{3+}. In particular, the Cd^{2+} adsorption experiments were carried out in the presence of 0.01 $mol·L^{-1}$, 0.05 $mol·L^{-1}$, and 0.1 $mol·L^{-1}$ concentrations of these three ions, respectively. In the presence of a 0.01 $mol·L^{-1}$ concentration of Na^+, the Cd^{2+} adsorption capacity of M60-HC was 5.3 times larger than that of HC (Table 2). Additionally, the presence of all three competing ions, Na^+, Ca^{2+}, and Al^{3+} in the Cd^{2+} solution had a negative impact on the Cd^{2+} adsorption onto hydrochar samples, with a significant difference of $P < 0.05$. The tested competitive ions, Na^+, Ca^{2+}, and Al^{3+}, interfered with the electrostatic attraction between Cd^{2+} ions and the adsorbent's surface. The highest shielding effect and inhibition of Cd^{2+} adsorption was associated with the presence of Na^+, followed by that of Ca^{2+} and Al^{3+}.

Table 3
Adsorption kinetic parameters and adsorption isothermal parameters of the process whereby Cd^{2+} is adsorbed onto various hydrochar samples.

Isotherm models	Langmuir			Freundlich				Temkin	
	Q_m (mg·g^{-1})	K_L (L·mg^{-1})	R^2	K_F mg$^{1-1/n}$L$^{-1/n}$·g^{-1}	1/n	R^2	A (L·g^{-1})	B	R^2
HC	4.19	0.034	0.990	0.280	0.586	0.989	0.296	0.972	0.975
M20-HC	8.88	0.026	0.988	0.368	0.695	0.981	0.230	2.112	0.941
M40-HC	19.90	0.015	0.997	0.444	0.762	0.993	0.231	3.146	0.986
M60-HC	20.18	0.120	0.996	2.903	0.372	0.922	1.314	2.777	0.966

Kinetic models	Parameter of Lagergren pseudo-first-order kinetic model			$Q_{e,exp}$ (mg·g^{-1})	Parameter of pseudo-second-order kinetic model		R^2
	$Q_{e,\ first}$ (mg·g^{-1})	K_1 (min^{-1})	R^2		$Q_{e,\ second}$ (mg·g^{-1})	K_2 mg·(g·min)$^{-1}$	
HC	1.35	0.028	0.985	2.13	2.18	0.052	0.896
M20-HC	1.55	0.045	0.971	2.76	3.26	0.077	0.953
M40-HC	1.94	0.067	0.958	4.56	4.73	0.154	0.904
M60-HC	2.53	0.077	0.984	9.02	9.64	0.352	0.984

Note: Lagergren pseudo-first-order rate equation is given as: $Q_t = Q_e(1\text{-}e^{-K_1 t})$, K_1 is the pseudo-first-order kinetic constant, $Q_{e,\ first}$ is the adsorption amount obtained by pseudo-first-order kinetic fitting; The pseudo-second-order rate equation is given as $Q_t = K_2 Q_e^2 t/(1 + K_2 Q_e t)$, K_2 is the adsorption rate constant, $Q_{e,\ second}$ is the adsorption amount obtained by pseudo-second-order kinetic fitting; The Langmuir equation is given as: $Q_e = Q_m K_L C_e/(1 + K_L C_e)$, Q_m is the theoretical saturated adsorption capacity (mg·g^{-1}), K_L is the Langmuir constant, which is related to adsorption energy (L·mg^{-1}); The Freundlich equation is given as: $Q_e = K_F C_e^{1/n}$, K_F is the Freundlich equation constant representing adsorption capacity, $1/n$ is the Freundlich equation constant; The Temkin equation is given as: $Q_e = B\ln A + B\ln C_e$,A and B are the Temkin constants.

3.3. Adsorption process and mechanism

3.3.1. Adsorption isotherm and kinetics

As can be seen from the data reported in Fig. 2c and Table 3, the Langmuir model best fitted the data ($R^2 > 0.988$), indicating a monolayer homogeneous Cd^{2+} adsorption (Zhou et al., 2018). The regression parameters of these models are listed in Table 3. Q_m corresponds to the maximum amount of adsorbate that can be adsorbed on a unit mass of the adsorbent. The Q_m value increased in the following order: HC < M20-HC < M40-HC < M60-HC (4.19, 8.88, 19.90, and 20.18 mg·g^{-1}, respectively) for Langmuir adsorption. Notably, the value of K_L (the parameter indicated by the Langmuir model corresponding to the ratio of adsorption to desorption rate) also increased as the hydrochar aging time increased; therefore, the adsorption ability of adsorbents also increased with hydrochar aging time. Up to now, only a few studies reported the adsorption process of heavy metals on hydrochars and their modified products. Shi et al. (2018) modified corn cob hydrochar with polyethylene imine (PEI), and the maximum adsorption capacities for Cr (VI) (33.66 mg·g^{-1}) and Ni (II) (29.06 mg·g^{-1}) on the modified hydrochars were 365% and 437% higher, respectively, than those on the unmodified hydrochar. Liu et al. (2018) reported that hydrochar chemically oxidized by $K_2Cr_2O_7$ and H_2O_2, and the adsorption capacity for Cd^{2+} reached 1.6 mg·g^{-1} and 4.0 mg·g^{-1}, respectively. Compared with these two approaches, in our study, the microbial aging process showed positive effect on Cd^{2+} adsorption, and the adsorption capacity of Cd^{2+} by microbial aged hydrochar was quite high. Besides, the microbial aging method is more environmentally friendly than conventional chemical modification method and easy to operate without complicated chemical reaction process.

The Lagergren pseudo-first-order and pseudo-second-order kinetic models were employed to fit the data reflecting the time-dependent variation of Cd^{2+} concentration and thus provide insight into the reaction pathway of the adsorption process (Fig. 2d). The experimental results reported in Table 3 indicate that Cd^{2+} adsorption by hydrochar in a Cd^{2+} solution of 50 mg·L^{-1} concentration reached its maximum value and equilibrium in 90 min. A correlation coefficient of > 0.896 was determined for the pseudo-first-order kinetic equation and the pseudo-second-order kinetic equation. The $Q_{e,exp}$ of the pseudo-first-order kinetic equation gradually increased with the aging time of the hydrochar. Although the behavior of all four hydrochar samples was well fitted by both kinetic models, the second-order kinetic equation had a higher fitting coefficient ($R^2 > 0.95$) and $Q_{e,second}$ values closer to their experimental counterparts. These results indicate the Cd^{2+} adsorption by HC, M20-HC, M40-HC, and M60-HC had the characteristics of chemisorption (Asl et al., 2017).

3.3.2. Thermodynamics of adsorption

In order to deduce the adsorption mechanism, a thermodynamic study of Cd^{2+} adsorption on the surface of different hydrochar samples was carried out. Notably, the hydrochar and cadmium ions interact at a solid–liquid interface, to which Cd^{2+} ions migrate from the liquid phase. At equilibrium, the chemical potential of Cd^{2+} ions in the liquid phase is the same as that of Cd^{2+} ions at the solid–liquid interface (Batool et al., 2018).

As can be evinced from the data in Table 4, the forces involved in Cd^{2+} adsorption by the hydrochar can be inferred from the enthalpy change associated with the said adsorption process. The positive enthalpy change associated with Cd^{2+} adsorption indicates an endothermic process. The positive entropy changes are indicative of a

Table 4
Thermodynamic parameters of Cd^{2+} adsorption onto different hydrochar samples.

Hydrochars	Temperature (K)	ΔG^0	ΔH^0	ΔS^0	R^2
		(KJ·mol^{-1})	(KJ·mol^{-1})	[J·(mol·K)$^{-1}$]	
HC	278.15	−21.02	2.82	65.38	0.761
	298.15	−19.73			
	318.15	−23.56			
M20-HC	278.15	−19.73	3.24	81.82	0.941
	298.15	−19.17			
	318.15	−21.65			
M40-HC	278.15	−18.95	2.98	34.93	0.879
	298.15	−19.82			
	318.15	−20.12			
M60-HC	278.15	−22.12	3.64	45.78	
	298.15	−21.87			0.765
	318.15	−20.98			

Note: The equation used for calculations includes apparent Gibbs free energy change (ΔG_0), apparent enthalpy change (ΔH^0), and apparent entropy change (ΔS^0): $\Delta G^0 = -RT\ln K$, $LnK = -\Delta H^0/RT + S^0/R$, $\Delta G^0 = \Delta H^0\text{-}T\Delta S^0$. the temperature is set to 278.15 K, 298.15 K, or 318.15 K; ΔG^0 is the apparent Gibbs free energy (KJ·mol^{-1}); ΔH^0 is the apparent enthalpy change (KJ·mol^{-1}); ΔS^0 is the apparent enthalpy change [J·(mol·K)$^{-1}$].

degree of disorder at the solid–liquid system (Wang et al., 2018).

The negative Gibbs free energies associated with Cd^{2+} adsorption onto HC, M20-HC, M40-HC, and M60-HC confirm that Cd^{2+} adsorption by the different hydrochar samples was a highly spontaneous process. In particular, the larger the absolute value of the Gibbs free energy, the more thermodynamically favorable the adsorption process. The calculation of the $\triangle G^0$ value associated with the adsorption process provides the means to acquire an insight into the mechanism by which cadmium ions are adsorbed onto the hydrochar. As mentioned above, a positive ΔS^0 value is indicative of the degree of disorder in the adsorption system. Cd^{2+} changes from the dissolved state in the solution to the adsorbed state on the adsorbent is a disordered increase process, which may be related to the fact that temperature rise is more conducive to the chemical adsorption of adsorbent for Cd^{2+}.

3.3.3. Summary of the adsorption mechanisms

The isothermal adsorption data conforms to the Langmuir model, indicating that it is homogeneous adsorption of monolayer, and the adsorption kinetic data conforms to the second-order kinetic model, indicating that it is chemisorption-dominated. And thermodynamic study showed that the adsorption process is endothermic and temperature has an important influence on the whole adsorption process. M−HC was observed much higher Cd^{2+} adsorption capacity than crude hydrochar HC, and the adsorption capacity was higher at longer aging time, which is due to the better developed porous structure through microbial process for M−HC.

Based on our results, it is proposed that Cd^{2+} adsorption onto both crude and microbially-aged hydrochar may have three possible mechanisms that were accountable for the adsorption process: (a) surface complexation, (b) electrostatics attraction and (c) cation exchange.

The first step of the adsorption process takes place the formation of a complex between Cd^{2+} and the oxygen-containing functional groups present on the hydrochar surface. The results of XPS analyses indicate that the number of –COOH and C = O groups on the hydrochar surface increased as a result of aging, subsequently increasing the oxidation degree of hydrochar. The results of the FTIR analyses suggest that chemical bonds are formed between –OH and Cd^{2+}, which weakened the hydrochar's intermolecular –OH based hydrogen bonding interactions. Cd^{2+} ion complexation by hydrochar also affects the position and appearance of the stretching and vibration absorption peaks of the –OH, C = C, C = O, and –COOH groups, confirming their role in Cd^{2+} adsorption. The shift in the Si-O-Si absorption peak from 781 cm^{-1} to 801 cm^{-1}, as a consequence of Cd^{2+} adsorption, indicates that Si-O-Si functional groups also provide adsorption sites for Cd^{2+} on the hydrochar surface. These results are consistent with the evidence reported by Gao et al. (2019). The formation of Cd^{2+} complexes via the π electrons, C = O, and C = N groups is also an important mechanism in heavy metal adsorption (Wang et al., 2017). The increase in the C = H and C = C functional group indicates that it is likely to coordinate with π bond to improve the adsorption capacity of Cd^{2+} (Cui et al., 2016).

Electrostatic interactions also play an important role in the mechanism whereby Cd^{2+} ions are adsorbed onto hydrochar. The zeta potential values of hydrochar HC was 0.37 mV, while the M−HC changed dramatically to −18.20 mV. As is known, the higher the absolute value of zeta potential, the more stable of the hydrochar system. After aging process, the M−HC became more stable, which is beneficial to Cd^{2+} adsorption. In particular, the negative zeta potential of M−HC means its surface was negatively charged under neutral pH, and will facilitate Cd^{2+} adsorption. Meanwhile, the pH of the hydrochar surface changed from acidic to alkaline after aging. Several previous studies indicated that physical properties of biochar such as surface porosity and chemical properties such as high pH, CEC, and various surface functional groups could increase Cd^{2+} immobilization through adsorption and complexation (Ahmad et al., 2014; Zeng et al., 2019). In addition, these researches explained that surface electronegative charges could increase Cd^{2+} adsorption through electrostatic interaction between Cd^{2+} and biochar surface charges. Similarly, in this study, microbial aging process also dramatically affected the zeta potential and pH of the hydrochar surface, which will enhance the electrostatic interactions between the negatively charged groups on the surface of hydrochar and the positively charged Cd^{2+} ions in the solution (Xu et al., 2016).

The presence of metal ions such as calcium and magnesium in the microbially-aged hydrochar water extract confirms that cation exchange also plays a role in the adsorption of Cd^{2+} (Tang et al., 2019). Because when a cation such as magnesium ion was detached from the M−HC surface, it means that a new adsorption site can be combined with the Cd^{2+} ion, which will lead to a higher adsorption capacity. These phenomena suggest that ion exchange between the Cd^{2+} and common exchangeable cations (Ca^{2+}, Mg^{2+}, and Al^{3+}) is an important mechanism for the removal of heavy metal from aqueous solutions by hydrochar. This result was in line with previous report by Harvey et al. (2011).

4. Conclusion

This study indicated that, following microbially aging process, both specific surface area and pore volume of hydrochar increased, which improved Cd^{2+} adsorption capacity by 3.8-fold at best. Moreover, the intensity of functional groups, such as –COOH, increased after aging. The adsorption of Cd^{2+} mainly due to the electrostatic interaction and functional group complexation, the auxiliary effect of cation exchange, and the coordination of heavy metal ions by way of π electrons. The kinetic study suggested that chemisorption is the dominant driver of the observed adsorption process. According to the thermodynamic data, Cd^{2+} adsorption by hydrochar is an endothermic process.

Funding

This research is funded by National Key Research and Development Program of China (2018YFD0800206); the National Natural Science Foundation of China (41877090, 31901195); Major Science and Technology Program for Water Pollution Control and Treatment (2017ZX07202004-003), Shandong Provincial Natural Science Foundation (ZR2019BD062) and NSF (CBET 1739884).

Declaration of Competing Interest

The authors declare that they have no known competing financial interests or personal relationships that could have appeared to influence the work reported in this paper.

Acknowledgments

The contribution of Dr. Hongbiao Cui from Anhui University of Science and Technology is highly appreciated. Feng Y. gratefully thanks the financially support from JAAS to study as a post doctor in University of Massachusetts, Amherst.

Appendix A. Supplementary data

Supplementary data to this article can be found online at https://doi.org/10.1016/j.biortech.2019.122708.

References

Ahmad, M., Rajapaksha, A.U., Lim, J.E., Zhang, M., Bolan, N., Mohan, D., Vithanage, M., Lee, S.S., Ok, Y.S., 2014. Biochar as a sorbent for contaminant management in soil and water: A review. Chemosphere. 99, 19–33.

Asl, S.M., Masomi, H., Hosseini, M., Javadian, M., Ruiz, H.M., Sastre, A.M., 2017. Synthesis of hydrous iron oxide/aluminum hydroxide composite loaded on coal fly ash as an effective mesoporous and low-cost sorbent for Cr(VI) sorption: fuzzy logic modeling. Process. Saf. Environ. 107, 153–167.

Aster, A., Wang, S.H., Mirmohades, M., Esmieu, C., Berggren, G., Hammarstrom, L., Lomoth, R., 2019. Metal vs. ligand protonation and the alleged proton-shuttling role of the azadithiolate ligand in catalytic H-2 formation with FeFe hydrogenase model complexes. Chem. Sci. 10 (21), 5582–5588.
Bai, W.B., Fan, L.R., Zhou, Y., Zhang, Y., Shi, J.Y., Lv, G.H., Wu, Y.F., Liu, Q., Song, J.Q., 2017. Removal of Cd^{2+} ions from aqueous solution using cassava starch-based superabsorbent polymers. J. Appl. Polym. Sci. 134 (17).
Batool, F., Akbar, J., Iqbal, S., Noreen, S., Bukhari, S.N.A., 2018. Study of isothermal, kinetic, and thermodynamic parameters for adsorption of cadmium: an overview of linear and nonlinear approach and error analysis. Bio. Chem. Appl. 2018, 1–11.
Brose, D.A., James, B.R., 2013. Hexavalent chromium reduction by tartaric acid and isopropyl alcohol in mid-atlantic soils and the role of Mn(III, IV)(hydr)oxides. Environ. Sci. Technol. 47 (22), 12985–12991.
Cortes-Arriagada, D., 2017. Adsorption of polycyclic aromatic hydrocarbons onto graphyne: comparisons with graphene. Int. J. Quantum. Chem. 117 (7).
Cui, H.B., Zhang, W., Zhou, J., Xu, L., Zhang, X., Zhang, S.W., Zhou, J., 2018. Availability and vertical distribution of Cu, Cd, Ca, and P in soil as influenced by lime and apatite with different dosages: a 7-year field study. Environ. Sci. Pollut. R. 25 (35), 35143–35153.
Cui, X.Q., Fang, S.Y., Yao, Y.Q., Li, T.Q., Ni, Q.J., Yang, X.E., He, Z.L., 2016. Potential mechanisms of cadmium removal from aqueous solution by canna indica derived biochar. Sci. Total. Environ. 562, 517–525.
Desplanques, V., Cary, L., Mouret, J.C., Trolard, F., Grauby, G., Meunier, J.D., 2006. Silicon transfers in a rice field in Camargue (France). J. Geochem. Explor. 88 (1–3), 190–193.
Epstein, E., 2009. Silicon: its manifold roles in plants. Ann. Appl. Biol. 155 (2), 155–160.
Feng, Y.F., Sun, H.J., Han, L.F., Xue, L.H., Chen, Y.D., Yang, L.Z., Xing, B.S., 2019. Fabrication of hydrochar based on food waste (FWHTC) and its application in aqueous solution rare earth ions adsorptive removal: process, mechanisms and disposal methodology. J. Clean. Prod. 212, 1423–1433.
Fosso-Kankeu, E., Waanders, H.F., Ray, S.S., 2017. Thermodynamic properties and adsorption behaviour of hydrogel nanocomposites for cadmium removal from mine effluents. J. Ind. Eng. Chem. 48, 151–161.
Gao, L.Y., Deng, J.H., Huang, G.F., Cai, Li, K., Liu, Y., Huang, F., 2019. Relative distribution of Cd^{2+} adsorption mechanisms on biochars derived from rice straw and sewage sludge. Bioresour. Technol. 272, 114–122.
Gayathri, R., Gopinath, K.P., Kumar, P.S., Suganya, S., 2019. Adsorption capability of surface-modified jujube seeds for Cd(II), Cu(II) and Ni(II) ions removal: mechanism, equilibrium, kinetic and thermodynamic analysis. Desalin. Water. Treat. 140, 268–282.
Harvey, O.R., Herbert, B.E., Rhue, R.D., Kuo, L.J., 2011. Metal Interactions at the biochar-water interface: energetics and structure-sorption relationships elucidated by flow adsorption microcalorimetry. Environ. Sci. Technol. 45 (13), 5550–5556.
Henriques, B., Coppola, F., Monteiro, Pinto, R.J., Viana, T., Pretti, C., Soares, A., Freitas, R., Pereira, E., 2019. Toxicological assessment of anthropogenic gadolinium in seawater: biochemical effects in mussels mytilus galloprovincialis. Sci. Total. Environ. 664, 626–634.
Jian, X.M., Zhuang, X.Z., Li, B.S., Xu, X.W., Wei, Z.B., Song, Y.P., Jiang, E.C., 2018. Comparison of characterization and adsorption of biochars produced from hydrothermal carbonization and pyrolysis. Environ. Technol. Inno. 10, 27–35.
Kumar, P., Pournara, A., Kim, K.H., Bansal, V., Rapti, S., Manos, M.J., 2017. Metal-organic frameworks: challenges and opportunities for ion-exchange/sorption applications. Prog. Mater. Sci. 86, 25–74.
Liu, Y., Ma, S., Chen, J., 2018a. A novel pyro-hydrochar via sequential carbonization of biomass waste: preparation, characterization and adsorption capacity. J. Clean. Prod. 176, 187–195.
Langova, S., Matysek, D., 2010. Zinc recovery from steel-making wastes by acid pressure leaching and hematite precipitation. Hydrometallurgy 101 (3–4), 171–173.
Liu, Y.X., Sun, B., Zheng, X.F., Yu, L.F., Li, J.G., 2018b. Integrated microwave and alkaline treatment for the separation between hemicelluloses and cellulose from cellulosic fibers. Bioresour. Technol. 247, 859–863.
Nessim, R.B., Bassiouny, A.R., Zaki, H.R., Moawad, M.N., Kandeel, K.M., 2011. Biosorption of lead and cadmium using marine algae. Chem. Ecol. 27 (6), 579–594.
Parshetti, G.K., Chowdhury, S., Balasubramanian, R., 2015. Biomass derived low-cost microporous adsorbents for efficient CO_2 capture. Fuel 148, 246–254.
Patel, B., Guo, M., Izadpanah, A., Shah, N., Hellgardt, K., 2016. A review on hydrothermal pre-treatment technologies and environmental profiles of algal biomass processing. Bioresour. Technol. 199, 288–299.
Qian, L.B., Chen, B.L., 2013. Dual role of biochars as adsorbents for aluminum: the effects of oxygen-containing organic components and the scattering of silicate particles. Environ. Sci. Technol. 47 (15), 8759–8768.
Qian, L.B., Chen, B.L., 2014. Interactions of aluminum with biochars and oxidized biochars: implications for the biochar aging process. J. Agr. Food. Chem. 62 (2), 373–380.
Rawat, A.P., Singh, D.P., 2019. Synergistic action of adsorption and reductive properties of ash derived from distilled mentha piperita plant waste in removal of Cr(VI) from aqueous solution. Ecotox. Environ. Safe 176, 27–33.
Rechberger, M.V., Kloss, S., Rennhofer, H., Tintner, J., Watzinger, A., Soja, G., Lichtenegger, H., Zehetner, F., 2017. Changes in biochar physical and chemical properties: accelerated biochar aging in an acidic soil. Carbon 115, 209–219.
Shi, Y.J., Zhang, T., Ren, H.Q., Kruse, A., Cui, R.F., 2018. Polyethylene imine modified hydrochar adsorption for chromium (VI) and nickel (II) removal from aqueous solution. Bioresour. Technol. 247, 370–379.
Bolisetty, S., Peydayesh, M., Mezzenga, R., 2019. Sustainable technologies for water purification from heavy metals: review and analysis. Chem. Soc. Rev. 2019 (48), 463–487.
Tang, C.L., Sun, P.F., Yang, J.L., Huang, Y.P., Wu, Y.H., 2019. Kinetics simulation of Cu and Cd removal and the microbial community adaptation in a periphytic biofilm reactor. Bioresour. Technol. 276, 199–203.
Usman, M., Chen, H.H., Chen, K.F., Ren, S., Clark, J.H., Fan, J.J., Luo, G., Zhang, S.C., 2019. Characterization and utilization of aqueous products from hydrothermal conversion of biomass for bio-oil and hydro-char production: a review. Green. Chem. 21 (7), 1553–1572.
Wang, J.L., Wang, S.Z., 2019. Preparation, modification and environmental application of biochar: a review. J. Clean. Prod. 227, 1002–1022.
Wang, N., Jin, R.N., Omer, A.M., Ouyang, X.K., 2017. Adsorption of Pb(II) from fish sauce using carboxylated cellulose nanocrystal: isotherm, kinetics, and thermodynamic studies. Int. J. Biol. Macromol. 102, 232–240.
Wang, S., Feng, Q.H., Zha, M., Javadpour, F., Hu, Q.H., 2018. Supercritical methane diffusion in shale nanopores: effects of pressure, mineral types, and moisture content. Energy. Fuels. 32 (1), 169–180.
Wu, Y.H., Yang, J.L., Tang, J., Kerr, P., Wong, P.K., 2017. The remediation of extremely acidic and moderate pH soil leachates containing Cu(II) and Cd (II) by native periphytic biofilm. J. Clean. Prod. 162, 846–855.
Xu, X.Y., Schierz, A., Xu, N., Cao, X.D., 2016. Comparison of the characteristics and mechanisms of Hg(II) sorption by biochars and activated carbon. J. Colloid. Interf. Sci. 463, 55–60.
Yoshida, N., Hirota, Y., Uchida, Asada, Y., Kobayashi, N.T., Nishiyama, N., 2018. Solvent-free synthesis and KOH activation of mesoporous carbons using resorcinol/Pluronic F127/hexamethylenetetramine mixture and their application to EDLC. Micropor. Mesopor. Mats. 272, 217–221.
Yu, S., Feng, Y.F., Xue, L.H., Sun, H.J., Han, L.F., Yang, L.Z., Sun, Q.Y., Chu, Q.N., 2019. Biowaste to treasure: application of microbial-aged hydrochar in rice paddy could improve nitrogen use efficiency and rice grain free amino acids. J. Clean. Prod. 240, 118180.
Yu, W.C., Lian, F., Cui, G.N., Liu, Z.Q., 2018. N-doping effectively enhances the adsorption capacity of biochar for heavy metal ions from aqueous solution. Chemosphere 193, 8–16.
Zama, E.F., Reid, B.J., Sun, G.X., Yuan, H.Y., Li, X.M., Zhu, Y.G., 2018. Silicon (Si) biochar for the mitigation of arsenic (As) bioaccumulation in spinach (Spinacia oleracean) and improvement in the plant growth. J. Clean. Prod. 189, 386–395.
Zeng, L., Lin, X., Zhou, F., Qin, J., Li, H., 2019. Biochar and crushed straw additions affect cadmium absorption in cassava-peanut intercropping system. Ecotox. Environ. Safe. 167, 520–530.
Zhang, C., Zeng, G.M., Huang, D.L., Lai, C., Chen, M., Cheng, M., Tang, W.W., Tang, L., Dong, H.R., Huang, B.B., Tan, X.F., Wang, R.Z., 2019a. Biochar for environmental management: mitigating greenhouse gas emissions, contaminant treatment, and potential negative impacts. Chem. Eng. J. 373, 902–922.
Zhao, Y.Q., Xu, C.F., Ai, S.Q., Wang, H.P., Gao, Y.M., Yan, L., Mei, Z.L., Wang, W., 2019. Biological pretreatment enhances the activity of functional microorganisms and the ability of methanogenesis during anaerobic digestion. Bioresour. Technol. 290, 121660.
Zhou, B.B., Feng, Y.F., Wang, Y.M., Yang, L.Z., Xue, L.H., Xing, B.S., 2018. Impact of hydrochar on rice paddy CH_4 and N_2O emissions: a comparative study with pyrochar. Chemosphere 204, 474–482.
Zhu, X.D., Liu, Y.C., Li, L.J., Shi, Q., Hou, J.Y., Zhang, R.X., Zhang, S.C., Chen, J.M., 2019. Nonthermal air plasma dehydration of hydrochar improves its carbon sequestration potential and dissolved organic matter molecular characteristics. Sci. Total. Environ. 659, 655–663.
Zhang, H.-M., Geng, G., Wang, J.-J., Xin, Y., Zhang, Q., Cao, D.-J., Ma, Y.-H., 2019b. The remediation potential and kinetics of cadmium in the green alga cladophora rupestris. Environ. Sci. Pollut. R 26 (1), 775–783.